

Relative Motion Estimation for Vision-based Formation Flight using Unscented Kalman Filter

Seung-Min Oh* and Eric N. Johnson †

School of Aerospace Engineering, Georgia Institute of Technology, Atlanta, GA 30332

This paper describes a vision-based relative motion estimator in the formation flight of two unmanned aerial vehicles (UAV's). The navigation of a follower aircraft relative to a target (or leader) aircraft is performed by vision-only information from a single camera fixed to the follower aircraft. The images of the target aircraft projected on the video-camera plane of the follower aircraft are captured and processed into vision information. The vision information for the relative motion estimator in this work is composed of three target angles: an azimuth angle, an elevation angle, and a subtended angle. Using this vision information measurement, the follower aircraft estimates a target relative position, a target relative velocity, a target size, and target acceleration components in the framework of an unscented Kalman filter (UKF). The UKF is applied to the relative motion estimator due to the highly nonlinear characteristics of the problem at hand. In order to evaluate the performance of the vision-based navigation filter, vision information obtained through a real-time flight test is post-processed by the filter. The real-time vision information, obtained by a geometric active contour method on an onboard computer, is composed of three points of the target aircraft on the camera image plane of the follower aircraft. These target points are the center point, the left wingtip point, and the right wingtip point. The target center point on the image plane provides information about the azimuth and the elevation angles of the target in the camera frame, and the two wingtip points provide information about the subtended angle of the target, which ultimately provides the target size. The vision-based estimation results of the target-follower relative motion and target characteristics are compared to actual data that are independently obtained from the onboard integrated navigation systems of both aircraft during the flight test. Each integrated navigation system is composed of an inertial measurement unit (IMU), a global positioning system (GPS), and a magnetometer. Comparisons indicate that the vision-based estimation filter produces satisfactory estimation results and thus successfully overcomes the highly nonlinear system characteristics by the UKF framework.

Nomenclature

\mathbf{a}^n	acceleration vector of a leader or a target relative to a follower in a navigation frame, $\mathbf{a}^n \triangleq \mathbf{a}_{L/F}^n = \mathbf{a}_L^n - \mathbf{a}_F^n$
\mathbf{a}_F^n	acceleration vector of a follower in a navigation frame
\mathbf{a}_L^n	acceleration vector of a leader or a target in a navigation frame
a_{lat}	lateral acceleration of a leader or a target in the y^c direction of a camera frame
a_{long}	longitudinal acceleration of a leader or a target in the z^c direction of a camera frame
b	leader or target size
\mathbf{C}_b^n	direction cosine matrix (DCM) or transformation matrix from a body frame to a navigation frame
\mathbf{C}_n^c	direction cosine matrix (DCM) or transformation matrix from a navigation frame to a camera frame
f	focal length of a pinhole camera
h	altitude
\mathbf{H}	Earth magnetic field
\mathbf{q}	quaternion vector
\mathbf{r}^c	position vector of a leader or a target relative to a follower in a camera frame, $\mathbf{r}^c = [X_c Y_c Z_c]^T$

*Graduate Research Assistant, Student Member AIAA, gtg895i@mail.gatech.edu.

†Lockheed Martin Associate Professor of Avionics Integration, Member AIAA, Eric.Johnson@ae.gatech.edu

\mathbf{r}^n	position vector of a leader or a target relative to a follower in a navigation frame, $\mathbf{r}^n \triangleq \mathbf{r}_{L/F}^n = \mathbf{r}_L^n - \mathbf{r}_F^n$
\mathbf{r}_F^n	position vector of a follower in a navigation frame
\mathbf{r}_L^n	position vector of a leader or a target in a navigation frame
n_{alat}	noise in a target lateral acceleration equation
n_{along}	noise in a target longitudinal acceleration equation
n_b	noise in a target size equation
\mathbf{n}_a	noise vector in a relative velocity equation
\mathbf{n}_v	noise vector in a relative position equation
\mathbf{v}^n	velocity vector of a leader or a target relative to a follower in a navigation frame, $\mathbf{v}^n \triangleq \mathbf{v}_{L/F}^n = \mathbf{v}_L^n - \mathbf{v}_F^n$
\mathbf{v}_F^n	velocity vector of a follower in a navigation frame
\mathbf{v}_L^n	velocity vector of a leader or a target in a navigation frame, $\mathbf{v}_L^n = \mathbf{v}_F^n + \mathbf{v}^n = [U_L \ V_L \ W_L]^T$
\mathbf{x}	state vector
\mathbf{y}	measurement vector
α	subtended angle
γ_y	azimuth angle
γ_z	elevation angle

Subscript or Superscript

0	initial condition at time $t = t_0 = 0$
b	body frame
c	camera frame
k	time index
m	measurement
n	navigation frame
F	follower
L	leader or target
L/F	leader or target relative to a follower
$\hat{(\)}$	estimated quantity of ()

I. Introduction

RECENTLY, the subject of unmanned aerial vehicles (UAV's) has been the focus of significant research interest in both military and commercial areas since they have a variety of practical applications, including reconnaissance, surveillance, target acquisition, search and rescue, patrolling, real-time monitoring, and mapping, to name a few.¹⁻⁵ To increase the autonomy and the capability of these UAV's and thus to reduce the workload of human operators, a typical UAV navigation system is equipped with various sensors among which a low-cost, MEMS-based GPS/IMU combination generally becomes a main navigation system and is aided by several other sensor systems, depending on the mission of each UAV.⁶ The main navigation system provides basic ownship states (typically inertial position, inertial velocity, and attitude) necessary for an autopilot system, and the aiding sensor systems provide other information (e.g., relative position and/or relative velocity with respect to a surrounding environment) necessary for their missions. Recently, one of the most attractive sensor systems is the vision system, typically a combination of a video camera, camera-image capturing hardware, and captured-image processing software.⁷ Indeed, the vision system has played a very important role in some applications and thus is used not just as an aiding sensor system but as one of the key elements determining guidance and control commands.⁸⁻¹³

The use of a vision sensor is very efficient due to its compact size and reduced cost while providing rich information. In addition, it is natural in that many living creatures including humans, animals, birds, and insects, when moving or navigating, primarily depend on their eyes or vision systems. The vision sensors are especially useful when the mission of UAV's is related to the tracking of other moving objects or the awareness of the global environment in which they fly.^{4,10,14} In fact, most of the recent UAV missions require both capabilities. On the other hand, one of the main impediments that make it difficult to use vision information is the computational burden for image-processing in order to extract useful information from the sequence of real-time images obtained from a camera or cameras. Nevertheless, recent progress in both hardware and software technology has made it feasible the use of vision systems in complicated UAV

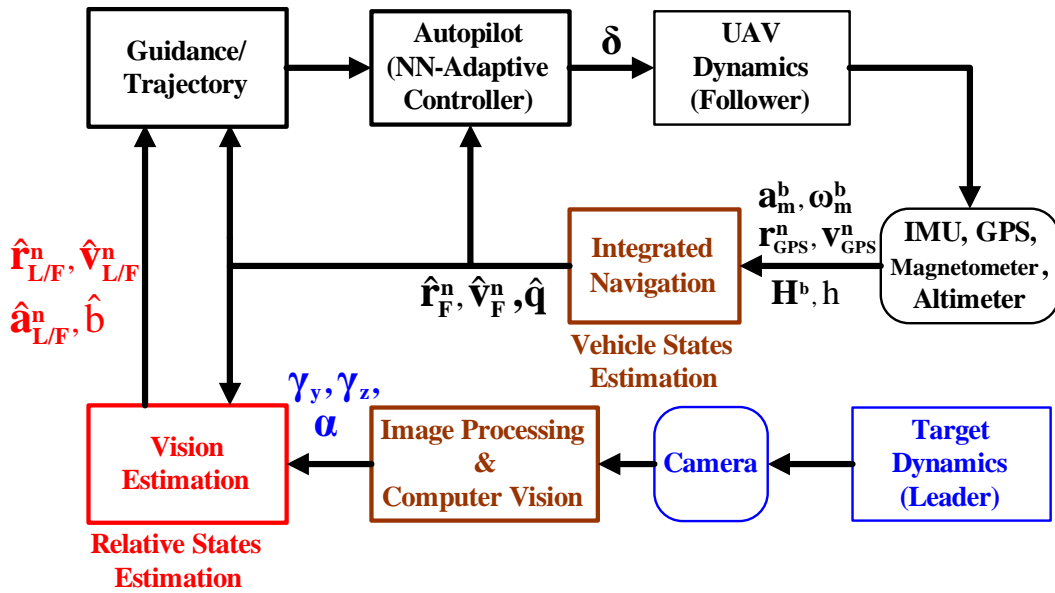


Figure 1. Closed-loop of Vision-based Navigation System for Leader/Follower Formation Flight

missions. In terms of hardware and software, first, a frame-grabber captures the sequence of high-rate images from the image stream of a video camera in real time, and then this sequence of images is image-processed and feature-extracted in an onboard computer by using recent computer vision algorithms such as geometric active contours.^{8,15} Finally, image processing is generally followed by a vision-based state estimator that extracts specific environment information depending on the sophistication of the UAV missions. The use of the vision-based estimation system in the closed-loop UAV GNC system of current work is presented in Figure 1. An accurate awareness of the surrounding environment depends on both the quality of the image processing outputs and the performance of the vision-based state estimator that estimates useful environment state information (e.g., a position and/or a velocity relative to obstacles or other vehicles) by using the image processing outputs as estimator measurement inputs. The details of the former, our image processing algorithm, are presented in related references,^{8,15,16} and thus, we limit our attention to the latter, our vision-based state estimator, in this work. Regarding the vision-based state estimator, the accuracy in the estimation of the surrounding environment including the relative location/velocity of stationary/moving obstacles and friendly/enemy vehicles is mostly crucial for ownship safety and/or complicated mission completion mainly because of the noisy and uncertain information about the environment. Related research applications are in the accurate estimation of the relative position and/or the relative velocity for the purpose of formation flight, target tracking, obstacle avoidance, trajectory planning, and the generation of advanced guidance and control commands.

In this paper, we consider the state estimation of relative motion in the scenario in which a follower UAV maintains some distance from a target aircraft based on vision-only information about the target. The estimated states are relative three-dimensional positions and velocities, a target size, and target acceleration components. We assume the follower UAV and the leader aircraft (or target) have no communication link.¹⁷ This generalization for no communication link makes the current work applicable to a variety of situations such as tracking or avoiding an adversarial air-target, flying in formation with communication loss when using the jamming- or spoofing-vulnerable GPS signals, and performing a silent, cooperative mission in an adversarial environment without being noticed by enemies. The governing equation of the estimation problem at hand is highly nonlinear because of the intrinsically involved complications of the problem. This problem is, in a sense, an extended version of a typical bearings-only problem.¹⁸⁻²⁰ The typical bearings-only problem, sometimes referred to as “target motion analysis” (TMA), is the estimation of the relative kinematics such as the relative position and velocity of a moving target in a planar motion using only noise-corrupted bearing measurements. Our problem, on the other hand, attempts to estimate not only relative kinematics such as relative position and velocity in three-dimensional space but also target characteristics such as target size and target acceleration components using two bearing angles and a subtended angle. Due to a variety of

important practical applications, even the relatively simple bearings-only problem has resulted in numerous research efforts in order to overcome the difficulty involved in inherent nonlinearity and observability issues. Those efforts include attempts to use effective coordinate systems such as modified polar coordinates^{18,21} and to apply various nonlinear filters such as unscented Kalman filters²² and particle filters.^{18,23} Recently, the unscented Kalman filter (UKF) has drawn much research attention mainly because of its several salient features.²⁴⁻²⁶ While maintaining the same order of magnitude in computational complexity, the UKF provides at least second-order accuracy compared to the first-order accuracy of the extended Kalman filter (EKF). In addition, the UKF does not necessitate the computation of the messy Jacobian matrices of a nonlinear process model and a measurement model, which is indispensable to apply the EKF.

The purpose of this research is to develop a vision-based navigation system^{1,27-30} that estimates relative kinematics and target characteristics based on vision-only information about the target in the framework of the UKF.⁷ The images of the target aircraft projected on the video-camera image plane of the follower aircraft are captured and processed into the vision information. The vision information for the relative motion estimator in this work is composed of three angles: a target azimuth angle, a target elevation angle, and a target subtended angle. Using this vision information measurement, the follower aircraft estimates the relative position, the relative velocity, the size, and the acceleration components of a target in the framework of the UKF. The UKF is applied to the relative motion estimator due to the highly nonlinear characteristics of the problem at hand. In order to evaluate the performance of the vision-based navigation filter, vision information obtained through a real-time flight test is post-processed by the filter. The real-time vision information, obtained by a geometric active contour method on an onboard computer, is composed of three points of the target aircraft on the camera image plane of the follower aircraft.¹⁵ These target points are the center point, the left wingtip point, and the right wingtip point. The target center point on the camera image plane provides information about the azimuth and the elevation angles of the target in the camera frame, and the two wing-tip points provide information about the subtended angle of the target that provides the target size. The vision-based estimation results of the target-follower relative motion and the target characteristics are compared to actual data independently obtained from the onboard integrated navigation systems of both aircraft during the flight test. Each integrated navigation system is composed of an IMU, a GPS, and a magnetometer. The current work is a part of independent research efforts to extend the capability of our previous vision-based state estimator based on an EKF.¹⁵ Even though the performance of the new vision-based estimator using the UKF is simulated in the scenario of a formation flight, this work can be easily applied to not only just flying in formation but also avoiding or pursuing other aircraft (e.g., stationary or moving obstacle avoidance, target tracking, evasive maneuvering). The developed algorithm is to be implemented on GTMax helicopter UAV³¹⁻³⁴ shown in Figure 2(a). A fixed-wing UAV, GTEdge, presented in Figure 2(b), is used as the target or leader aircraft whose image sequence on the image plane of the follower aircraft (GTMax) provides the real-time image information during the flight test.



Figure 2. GTMax and GTEdge UAV

The paper is organized as follows. Section II discusses the overall system description for vision-based

relative navigation and includes the details of a process model, a measurement model, and measurements from an image processor. Section III summarizes the UKF algorithm used in this work. Section IV presents the filter initializations of a state vector and a covariance matrix and the simulation results starting these initial conditions. Finally, section V summarizes the paper.

II. System Description for Vision-Based Relative Navigation

This section describes the formulation details of a vision-based relative motion estimator using an unscented Kalman filter (UKF). The state vector is composed of the relative position, the relative velocity, the size, and the lateral and longitudinal acceleration components of the target. Three target angles—the azimuth angle, the elevation angle, and the subtended angle—are used as the measurements obtained from the onboard image processor. By using the UKF, we are able to remove the rather messy step of calculating Jacobian matrices of the nonlinear process and measurement model.

A. Process Model of Vision-based Formation Flight

The state vector of the process model for the vision-based relative navigation includes three relative position components, three relative velocity components, a target (or leader) size, and target lateral and longitudinal acceleration components:

$$\mathbf{x} = \begin{bmatrix} x_{1:3} \\ x_{4:6} \\ x_7 \\ x_8 \\ x_9 \end{bmatrix} = \begin{bmatrix} \mathbf{r}^n \\ \mathbf{v}^n \\ b \\ a_{lat} \\ a_{long} \end{bmatrix}, \quad \text{where } \mathbf{r}^n = \begin{bmatrix} X \\ Y \\ Z \end{bmatrix}, \quad \mathbf{v}^n = \begin{bmatrix} U \\ V \\ W \end{bmatrix}. \quad (1)$$

Here, as represented in Figure 3, \mathbf{r}^n and \mathbf{v}^n are the relative position vector and the relative velocity vector from a follower vehicle to a leader or target vehicle in a navigation frame, respectively, b is the target or leader size, a_{lat} is the target or leader lateral acceleration, and a_{long} is the target or leader longitudinal acceleration.

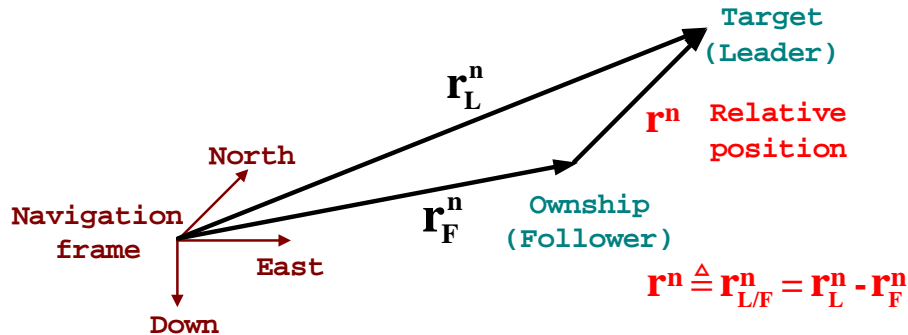


Figure 3. Leader/Follower Relative Position in a Navigation Frame

The continuous-time process model can be expressed by these state vector components. Since $\begin{bmatrix} x_1 \\ x_2 \\ x_3 \end{bmatrix} = \mathbf{r}^n = \begin{bmatrix} X \\ Y \\ Z \end{bmatrix}$, we have $\begin{bmatrix} \dot{x}_1 \\ \dot{x}_2 \\ \dot{x}_3 \end{bmatrix} = \dot{\mathbf{r}}^n = \mathbf{v}^n = \begin{bmatrix} x_4 \\ x_5 \\ x_6 \end{bmatrix} \triangleq \begin{bmatrix} f_1 \\ f_2 \\ f_3 \end{bmatrix}$. Similarly, using the fact that $\begin{bmatrix} x_4 \\ x_5 \\ x_6 \end{bmatrix} = \dot{\mathbf{r}}^n = \mathbf{v}^n = \begin{bmatrix} U \\ V \\ W \end{bmatrix}$, we have $\begin{bmatrix} \dot{x}_4 \\ \dot{x}_5 \\ \dot{x}_6 \end{bmatrix} = \ddot{\mathbf{r}}^n = \dot{\mathbf{v}}^n = \mathbf{a}^n = \begin{bmatrix} A_x \\ A_y \\ A_z \end{bmatrix} \triangleq \begin{bmatrix} f_4 \\ f_5 \\ f_6 \end{bmatrix}$.

Furthermore, $\dot{x}_7 = \dot{b} = 0 \triangleq f_7$, $\dot{x}_8 = \dot{a}_{lat} = 0 \triangleq f_8$, and $\dot{x}_9 = \dot{a}_{long} = 0 \triangleq f_9$. We assumed constant target size and constant target lateral/longitudinal acceleration. We need to express the relative acceleration, \mathbf{a}^n , as a function of state variables. Based on the assumptions that leader's longitudinal acceleration is perpendicular to the leader's total velocity and lies in the vertical plane generated by the total velocity vector and the vertical direction vector (W_L direction), and leader's lateral acceleration is also perpendicular to the leader's total velocity but lies in the horizontal plane, we can express the leader acceleration as a function of leader's velocity components as follows:³⁵

$$\mathbf{a}_L^n = \frac{1}{\sqrt{U_L^2 + V_L^2}} \begin{bmatrix} \frac{U_L W_L}{\sqrt{U_L^2 + V_L^2 + W_L^2}} & -V_L \\ \frac{V_L W_L}{\sqrt{U_L^2 + V_L^2 + W_L^2}} & U_L \\ -\frac{U_L^2 + V_L^2}{\sqrt{U_L^2 + V_L^2 + W_L^2}} & 0 \end{bmatrix} \begin{bmatrix} a_{long} \\ a_{lat} \end{bmatrix}, \quad (2)$$

where

$$\mathbf{v}_L^n = \begin{bmatrix} U_L \\ V_L \\ W_L \end{bmatrix} = \mathbf{v}^n + \mathbf{v}_F^n = \begin{bmatrix} x_4 \\ x_5 \\ x_6 \end{bmatrix} + \mathbf{v}_F^n. \quad (3)$$

\mathbf{a}_L^n is leader acceleration in the navigation frame, \mathbf{v}_L^n is leader velocity in the navigation frame, \mathbf{v}_F^n is follower velocity in the navigation frame, and \mathbf{v}^n is relative velocity vector from the follower vehicle to the leader vehicle in the navigation frame. \mathbf{v}_F^n is assumed to be known from the follower's navigation system. Using these facts, we can express relative acceleration as a function of state variable components.

$$\begin{bmatrix} f_4 \\ f_5 \\ f_6 \end{bmatrix} \triangleq \begin{bmatrix} A_x \\ A_y \\ A_z \end{bmatrix} = \mathbf{a}^n = \mathbf{a}_L^n - \mathbf{a}_F^n = \frac{1}{\sqrt{U_L^2 + V_L^2}} \begin{bmatrix} \frac{U_L W_L}{\sqrt{U_L^2 + V_L^2 + W_L^2}} & -V_L \\ \frac{V_L W_L}{\sqrt{U_L^2 + V_L^2 + W_L^2}} & U_L \\ -\frac{U_L^2 + V_L^2}{\sqrt{U_L^2 + V_L^2 + W_L^2}} & 0 \end{bmatrix} \begin{bmatrix} a_{long} \\ a_{lat} \end{bmatrix} - \mathbf{a}_F^n, \quad (4)$$

where the follower acceleration in the navigation frame, \mathbf{a}_F^n , is assumed to be known from the follower's navigation system.

Therefore, the process model for the vision-based formation flight in continuous-time state-space matrix form can be expressed as follows:

$$\dot{\mathbf{x}}(\mathbf{t}) = \mathbf{f}(\mathbf{x}(t)) + \mathbf{w}(t) \quad (5)$$

or

$$\begin{bmatrix} \dot{\mathbf{i}}^n \\ \dot{\mathbf{v}}^n \\ \dot{b} \\ \dot{a}_{lat} \\ \dot{a}_{long} \end{bmatrix} = \begin{bmatrix} \mathbf{v}^n \\ \mathbf{a}^n \\ 0 \\ 0 \\ 0 \end{bmatrix} + \begin{bmatrix} \mathbf{n}_v \\ \mathbf{n}_a \\ n_b \\ n_{alat} \\ n_{along} \end{bmatrix}, \quad (6)$$

where

$$\mathbf{v}^n = \begin{bmatrix} x_4 \\ x_5 \\ x_6 \end{bmatrix}, \quad \mathbf{a}^n = \mathbf{a}_L^n - \mathbf{a}_F^n = \frac{1}{\sqrt{U_L^2 + V_L^2}} \begin{bmatrix} \frac{U_L W_L}{\sqrt{U_L^2 + V_L^2 + W_L^2}} & -V_L \\ \frac{V_L W_L}{\sqrt{U_L^2 + V_L^2 + W_L^2}} & U_L \\ -\frac{U_L^2 + V_L^2}{\sqrt{U_L^2 + V_L^2 + W_L^2}} & 0 \end{bmatrix} \begin{bmatrix} x_9 \\ x_8 \end{bmatrix} - \mathbf{a}_F^n, \quad (7)$$

$$\begin{bmatrix} U_L \\ V_L \\ W_L \end{bmatrix} = \mathbf{v}_L^n = \mathbf{v}^n + \mathbf{v}_F^n = \begin{bmatrix} x_4 \\ x_5 \\ x_6 \end{bmatrix} + \mathbf{v}_F^n. \quad (8)$$

In matrix component form, we have

$$\dot{\mathbf{x}} = \begin{bmatrix} \dot{x}_1 \\ \dot{x}_2 \\ \dot{x}_3 \\ \dot{x}_4 \\ \dot{x}_5 \\ \dot{x}_6 \\ \dot{x}_7 \\ \dot{x}_8 \\ \dot{x}_9 \end{bmatrix} = \frac{1}{\sqrt{U_L^2 + V_L^2}} \begin{bmatrix} x_4 \\ x_5 \\ x_6 \\ \frac{U_L W_L}{\sqrt{U_L^2 + V_L^2 + W_L^2}} & -V_L \\ \frac{V_L W_L}{\sqrt{U_L^2 + V_L^2 + W_L^2}} & U_L \\ -\frac{U_L^2 + V_L^2}{\sqrt{U_L^2 + V_L^2 + W_L^2}} & 0 \\ 0 \\ 0 \\ 0 \end{bmatrix} \begin{bmatrix} x_9 \\ x_8 \end{bmatrix} - \mathbf{a}_F^n + \begin{bmatrix} \mathbf{n}_v \\ \mathbf{n}_a \\ n_b \\ n_{along} \end{bmatrix}, \quad (9)$$

where

$$\begin{bmatrix} U_L \\ V_L \\ W_L \end{bmatrix} = \mathbf{v}_L^n = \mathbf{v}^n + \mathbf{v}_F^n = \begin{bmatrix} x_4 \\ x_5 \\ x_6 \end{bmatrix} + \mathbf{v}_F^n. \quad (10)$$

Follower velocity \mathbf{v}_F^n and follower acceleration \mathbf{a}_F^n in the navigation frame are assumed to be known from the follower's (ownship) navigation system.

B. Measurement Model of a Vision-based Formation Flight

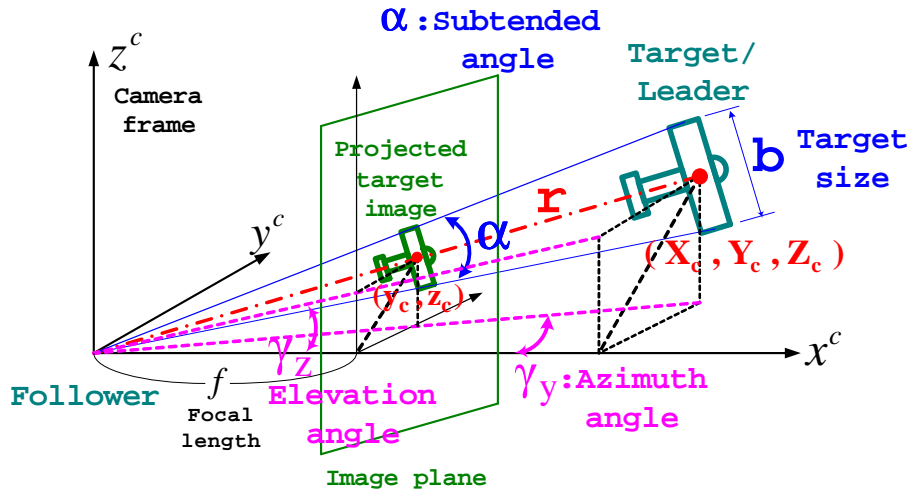


Figure 4. Projected Target Image on the Image Plane of a Pinhole Camera

For the measurement quantities, we use three target angles: an azimuth angle γ_y , an elevation angle γ_z , and a subtended angle α ,^{2,15} illustrated in Figure 4. These three angles have the following relationships:

$$\tan \gamma_y = \frac{Y_c}{X_c}, \quad (11)$$

$$\tan \gamma_z = \frac{Z_c}{X_c}, \quad (12)$$

$$\tan \frac{\alpha}{2} = \frac{b}{2r} = \frac{b}{2\sqrt{X_c^2 + Y_c^2 + Z_c^2}}, \quad (13)$$

where $\mathbf{r}^c = \begin{bmatrix} X_c \\ Y_c \\ Z_c \end{bmatrix} = C_n^c \begin{bmatrix} X \\ Y \\ Z \end{bmatrix} = C_n^c \begin{bmatrix} x_1 \\ x_2 \\ x_3 \end{bmatrix}$ is the target relative position in a camera frame, C_n^c is the transformation matrix from the navigation frame to the camera frame, which is given by the follower navigation system, and $r = \sqrt{X_c^2 + Y_c^2 + Z_c^2}$ is the relative distance between the follower aircraft and the leader aircraft. Now, we can express the three measurement angles as a function of state variables as follows:

$$\therefore \mathbf{y} = \begin{bmatrix} \gamma_y \\ \gamma_z \\ \alpha \end{bmatrix} = \begin{bmatrix} \tan^{-1} \left(\frac{Y_c}{X_c} \right) \\ \tan^{-1} \left(\frac{Z_c}{X_c} \right) \\ 2 \tan^{-1} \left(\frac{x_3}{2 \sqrt{X_c^2 + Y_c^2 + Z_c^2}} \right) \end{bmatrix}, \quad (14)$$

where $\begin{bmatrix} X_c \\ Y_c \\ Z_c \end{bmatrix} = \mathbf{r}^c = C_n^c \mathbf{r}^n = C_n^c \begin{bmatrix} x_1 \\ x_2 \\ x_3 \end{bmatrix}$, and C_n^c is assumed to be known from the follower's (ownship) navigation system.

C. Measurement from the Image Processor

From the image processor, we receive three target data points in the camera image plane: the center point (y_c, z_c) , the left wingtip point (y_l, z_l) , and the right wingtip point (y_r, z_r) .

Using the characteristics of a pinhole camera, we have the following relationships for the target azimuth angle and the target elevation angle:

$$\tan \gamma_y = \frac{y_c}{f} = \frac{Y_c}{X_c}, \quad (15)$$

$$\tan \gamma_z = \frac{z_c}{f} = \frac{Z_c}{X_c}, \quad (16)$$

where f is the focal length of a pinhole camera, (y_c, z_c) is the projected target center position on the camera

image plane, and $\mathbf{r}^c = \begin{bmatrix} X_c \\ Y_c \\ Z_c \end{bmatrix}$ is the relative target position in the camera frame. Since the relative distance

from the origin of the camera frame to the center point of the projected target image on the image plane is $\sqrt{f^2 + y_c^2 + z_c^2}$, and the projected target size on the image plane is $\sqrt{(y_l - y_r)^2 + (z_l - z_r)^2}$, the target subtended angle can be expressed as follows:

$$\tan \frac{\alpha}{2} = \frac{\sqrt{(y_l - y_r)^2 + (z_l - z_r)^2}}{2 \sqrt{f^2 + y_c^2 + z_c^2}} = \frac{b}{2r} = \frac{b}{2 \sqrt{X_c^2 + Y_c^2 + Z_c^2}}. \quad (17)$$

Now, the three angle measurements from the image processor are obtained as follows:

$$\therefore \mathbf{y} = \begin{bmatrix} \gamma_y \\ \gamma_z \\ \alpha \end{bmatrix} = \begin{bmatrix} \tan^{-1} \left(\frac{y_c}{f} \right) \\ \tan^{-1} \left(\frac{z_c}{f} \right) \\ 2 \tan^{-1} \left(\frac{\sqrt{(\frac{y_l}{f} - \frac{y_r}{f})^2 + (\frac{z_l}{f} - \frac{z_r}{f})^2}}{2 \sqrt{1 + (\frac{y_c}{f})^2 + (\frac{z_c}{f})^2}} \right) \end{bmatrix}. \quad (18)$$

III. Unscented Kalman Filter (UKF)

This section summarizes the unscented Kalman filter, first developed by Julier et al.^{25,36,37} and diversified into several algorithms by Merwe et al.^{26,38,39}

The general nonlinear discrete-time process model and discrete-time measurement model in a state-space form are given by

$$\mathbf{x}_{k+1} = \mathbf{f}_d(\mathbf{x}_k, \mathbf{u}_k, k) + \mathbf{w}_k, \quad \mathbf{w}_k \sim N(0, \mathbf{Q}_k), \quad (19)$$

$$\mathbf{y}_k = \mathbf{h}(\mathbf{x}_k, k) + \mathbf{v}_k, \quad \mathbf{v}_k \sim N(0, \mathbf{R}_k), \quad (20)$$

where initial conditions ($\mathbf{x}(t_0) \sim N(\hat{\mathbf{x}}_0, \mathbf{P}_0)$) are assumed to be known and have the following form:

$$\hat{\mathbf{x}}_0 = E[\mathbf{x}(t_0)], \quad (21)$$

$$\mathbf{P}_0 = E[(\mathbf{x}(t_0) - \hat{\mathbf{x}}_0)(\mathbf{x}(t_0) - \hat{\mathbf{x}}_0)^T]. \quad (22)$$

In order to apply the UKF, it is necessary to introduce a parameter and weights.²⁴ The constant γ , needed to determine the spread of sigma points around mean state value, is chosen such that $n + \lambda = 3$, and thus $\gamma = \sqrt{n + \lambda} = \sqrt{3}$. In addition, the following weights are used:

$$w_0^{(m)} = \frac{\lambda}{n + \lambda} = 1 - \frac{n}{\gamma^2}, \quad (23)$$

$$w_0^{(c)} = \frac{\lambda}{n + \lambda} = 1 - \frac{n}{\gamma^2}, \quad (24)$$

$$w_i^{(m)} = w_i^{(c)} = \frac{1}{2(n + \lambda)} = \frac{1}{2\gamma^2}, \quad i = 1, 2, \dots, 2n. \quad (25)$$

In order to start the standard UKF algorithm, we need to initialize $\hat{\mathbf{x}}_0$ and \mathbf{S}_0 as follows:

$$\hat{\mathbf{x}}_0 = E[\mathbf{x}_0], \quad (26)$$

$$\mathbf{P}_0 = E[(\mathbf{x}_0 - \hat{\mathbf{x}}_0)(\mathbf{x}_0 - \hat{\mathbf{x}}_0)^T], \quad (27)$$

$$\mathbf{S}_0 = \{chol(\mathbf{P}_0)\}^T. \quad (28)$$

Note that Matlab function ‘‘chol’’ provides Cholesky factorization in a upper triangular form, but it needs to be transposed to obtain \mathbf{S}_0 in a lower triangular form.

1. Time Update

For each time step $k = 1, 2, \dots$, we need first to calculate sigma points and then time-update using time-update equations.

• Sigma-point calculation

$$\mathbf{S}_{k-1} = \{chol(\mathbf{P}_{k-1})\}^T, \quad (29)$$

$$\mathbf{X}_{k-1} = [\hat{\mathbf{x}}_{k-1} \quad \hat{\mathbf{x}}_{k-1} + \gamma \mathbf{S}_{k-1} \quad \hat{\mathbf{x}}_{k-1} - \gamma \mathbf{S}_{k-1}]. \quad (30)$$

• Time-update equations

$$\mathbf{X}_{k|k-1}^* = \mathbf{f}_d(\mathbf{X}_{k-1}, \mathbf{u}_{k-1}), \quad (31)$$

$$\hat{\mathbf{x}}_k^- = \sum_{i=0}^{2n} w_i^{(m)} \mathbf{X}_{i,k|k-1}^*, \quad (32)$$

$$\mathbf{P}_k^- = \sum_{i=0}^{2n} w_i^{(c)} (\mathbf{X}_{i,k|k-1}^* - \hat{\mathbf{x}}_k^-)(\mathbf{X}_{i,k|k-1}^* - \hat{\mathbf{x}}_k^-)^T + \mathbf{Q}_k, \quad (33)$$

where $\mathbf{Q}_k = \Delta t \mathbf{Q}(t)$.

2. Measurement Update

• Augmented sigma points

$$\mathbf{S}_k^- = \{\text{chol}(\mathbf{P}_k^-)\}^T, \quad (34)$$

$$\mathbf{X}_{k|k-1} = [\hat{\mathbf{x}}_k^- \quad \hat{\mathbf{x}}_k^- + \gamma \mathbf{S}_k^- \quad \hat{\mathbf{x}}_k^- - \gamma \mathbf{S}_k^-], \quad (35)$$

$$\mathbf{Y}_{k|k-1} = \mathbf{h}(\mathbf{X}_{k|k-1}), \quad (36)$$

$$\hat{\mathbf{y}}_k^- = \sum_{i=0}^{2n} w_i^{(m)} \mathbf{Y}_{i,k|k-1}. \quad (37)$$

• Measurement-update equations

$$\mathbf{P}_y = \sum_{i=0}^{2n} w_i^{(c)} (\mathbf{Y}_{i,k|k-1} - \hat{\mathbf{y}}_k^-) (\mathbf{Y}_{i,k|k-1} - \hat{\mathbf{y}}_k^-)^T + \mathbf{R}_k, \quad (38)$$

$$\mathbf{P}_{xy} = \sum_{i=0}^{2n} w_i^{(c)} (\mathbf{X}_{i,k|k-1} - \hat{\mathbf{x}}_k^-) (\mathbf{Y}_{i,k|k-1} - \hat{\mathbf{y}}_k^-)^T, \quad (39)$$

$$\mathbf{K}_k = \mathbf{P}_{xy} \mathbf{P}_y^{-1}, \quad (40)$$

$$\hat{\mathbf{x}}_k = \hat{\mathbf{x}}_k^- + \mathbf{K}_k (\mathbf{y}_k - \hat{\mathbf{y}}_k^-), \quad (41)$$

$$\mathbf{P}_k = \mathbf{P}_k^- - \mathbf{K}_k \mathbf{P}_y \mathbf{K}_k^T. \quad (42)$$

IV. Simulation and Results

A. Initialization and Noise Covariance Setting

Filter initialization is performed by using the current measurement.

1) Initialization of the State Vector

$$\begin{bmatrix} x_1(t_0) \\ x_2(t_0) \\ x_3(t_0) \end{bmatrix} = \begin{bmatrix} X(t_0) \\ Y(t_0) \\ Z(t_0) \end{bmatrix} = C_c^n \begin{bmatrix} X_c(t_0) \\ Y_c(t_0) \\ Z_c(t_0) \end{bmatrix}, \quad (43)$$

$$\begin{bmatrix} x_4(t_0) \\ x_5(t_0) \\ x_6(t_0) \end{bmatrix} = \begin{bmatrix} 0 \\ 0 \\ 0 \end{bmatrix}, \quad (44)$$

$$x_7(t_0) = \hat{b}_0, \quad (45)$$

$$x_8(t_0) = 0.0, \quad (46)$$

$$x_9(t_0) = 0.0, \quad (47)$$

where

$$X_c = \frac{\hat{b}_0}{2 \tan \frac{\alpha}{2} \sqrt{1 + \tan^2 \gamma_y + \tan^2 \gamma_z}}, \quad (48)$$

$$Y_c = X_c \tan \gamma_y, \quad (49)$$

$$Z_c = X_c \tan \gamma_z. \quad (50)$$

($\hat{b}_0=8.75$ ft: estimate of leader wingspan or target size)

2) Initialization of the Error Covariance Matrix

$$P(t_0) = \text{diag}\{\sigma_X^2, \sigma_Y^2, \sigma_Z^2, \sigma_U^2, \sigma_V^2, \sigma_W^2, \sigma_b^2, \sigma_{alat}^2, \sigma_{along}^2\}, \quad (51)$$

where $\sigma_X = \sigma_Y = \sigma_Z = 1$ ft, $\sigma_U = \sigma_V = \sigma_W = 1$ ft/sec, $\sigma_b = 0.02 * \hat{b}_0$ ft, $\sigma_{alat} = 10$ ft/sec², $\sigma_{along} = 10$ ft/sec².

3) Process Noise

$$Q_k = \Delta t Q, \quad (52)$$

$$Q = \text{diag}\{\sigma_{\dot{X}}^2, \sigma_{\dot{Y}}^2, \sigma_{\dot{Z}}^2, \sigma_{\dot{U}}^2, \sigma_{\dot{V}}^2, \sigma_{\dot{W}}^2, \sigma_b^2, \sigma_{\dot{a}_{lat}}^2, \sigma_{\dot{a}_{long}}^2\}, \quad (53)$$

where $\sigma_{\dot{X}} = \sigma_{\dot{Y}} = \sigma_{\dot{Z}} = 5 \text{ ft/sec}$, $\sigma_{\dot{U}} = \sigma_{\dot{V}} = \sigma_{\dot{W}} = 10 \text{ ft/sec}^2$, $\sigma_b = 0.01 * \hat{b}_0 \text{ ft/sec}$, $\sigma_{\dot{a}_{lat}} = 2 \text{ ft/sec}^3$, $\sigma_{\dot{a}_{long}} = 2 \text{ ft/sec}^3$.

4) Measurement Noise

$$R = \text{diag}\{\sigma_{\gamma_y}^2, \sigma_{\gamma_z}^2, \sigma_{\alpha}^2\}, \quad (54)$$

where $\sigma_{\gamma_y} = 5 \text{ deg}$, $\sigma_{\gamma_z} = 4 \text{ deg}$, $\sigma_{\alpha} = 3 \text{ deg}$.

B. Simulation Results



Figure 5. GTMax and GTEdge in Formation Flight

This paper describes a vision-based relative motion estimator in the formation flight of two unmanned aerial vehicles (UAV's). We consider the state estimation of relative motion in the scenario in which a follower UAV (GTMax) maintains some distance from a target aircraft (GTEdge) based on vision-only information about the target (Figure 5(a)). The navigation of a follower aircraft relative to a target (or leader) aircraft is performed by vision-only information from a single camera fixed to the follower aircraft. The images of the target aircraft projected on the video-camera image plane of the follower aircraft are captured and processed into vision information. One typical image of the target aircraft captured by the follower aircraft is presented in Figure 5(b). Estimated states by using the image measurement are target relative position and velocity, target size, and target acceleration components. In order to evaluate the performance of the vision-based navigation filter, vision information obtained through a real-time flight test is post-processed by the filter. The real-time vision information, obtained by a geometric active contour method on an onboard computer, is composed of three points of the target aircraft on the camera image plane. These target points are the center point, the left wingtip point, and the right wingtip point in the camera image plane in Figures 6(a) and 6(b). Figure 6(c) shows the image registration status in which "1" denotes an image registered (success) and "0" denotes an image not registered (failure). The target center point on the camera image plane provides information about the azimuth and the elevation angles of the target in the camera frame, and the two wingtip points provide information about the subtended angle of the target, which ultimately provides the target size. Figure 7 represents three target angle measurements—the azimuth angle, the elevation angle, and the subtended angle—obtained by image processing outputs and used as the inputs to the filter. Using this vision information measurement, follower aircraft estimates the relative position, the relative velocity, the size, and the acceleration components of the target in the framework of an unscented Kalman filter (UKF). The UKF is applied to the relative motion estimator due to the highly nonlinear characteristics of the problem at hand.

The vision-based estimation results about the target-follower relative motion and target characteristics are compared to actual data that are independently obtained from the onboard integrated navigation systems of both aircraft during a flight test. The relative position, i.e., the target position relative to the follower position, in the navigation frame is presented in Figure 8. The relative position components of the vision-based estimator outputs are compared with the actual flight test results. The actual relative position components from the flight test are computed from the recorded data by the onboard navigation systems (mainly from the GPS/INS) of each aircraft. The actual positions of each aircraft are independently recorded during the flight test for comparison purposes. Similarly, relative velocity components and relative acceleration components of estimator outputs are compared with the flight test results, shown in the Figures 9 and 10, respectively. The amount of absolute error between the estimator outputs and flight test results for the relative position, the relative velocity, and the relative acceleration components are presented in Figures 11~13. Figure 14 compares the target characteristics of the truth and the estimator outputs in terms of the target size, the target lateral acceleration, and the target longitudinal acceleration. Figure 14(b) shows the rapid convergence in the estimation of the target lateral acceleration from 0 to around $8 \text{ ft}/\text{sec}^2$. Since the flight test was performed in nearly planar circular motion, the target lateral acceleration is nearly constant as a centripetal acceleration form, and the target longitudinal acceleration is approximately zero. Comparisons indicate that the vision-based estimation filter provides satisfactory estimation results and thus successfully overcomes the highly nonlinear system characteristics by the UKF framework.

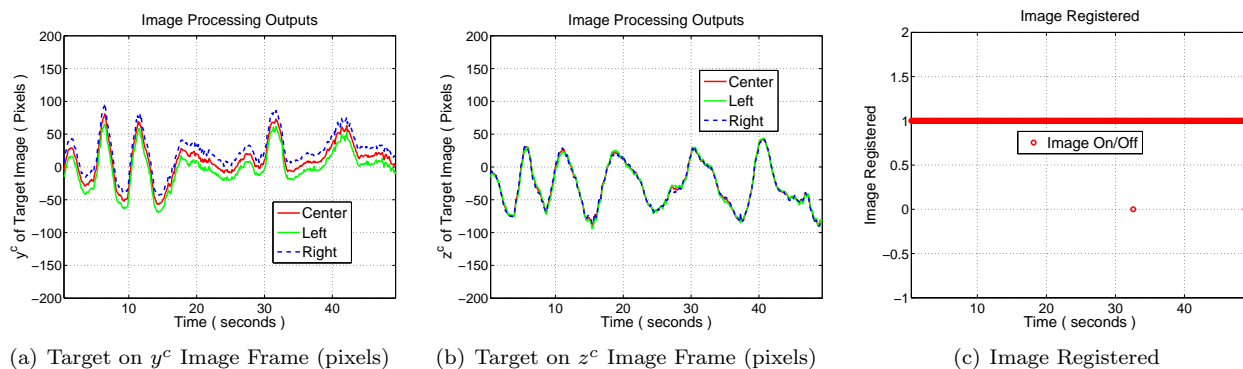


Figure 6. Image Processing Outputs of the Target Position

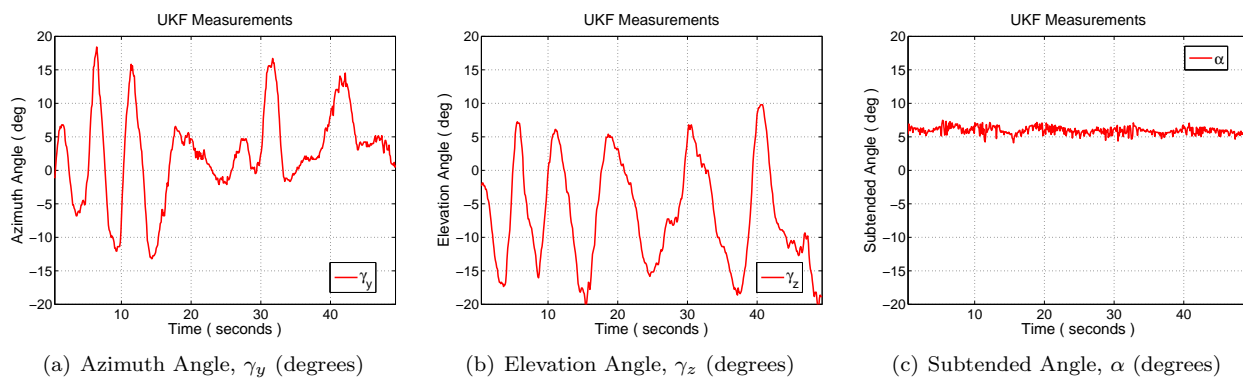
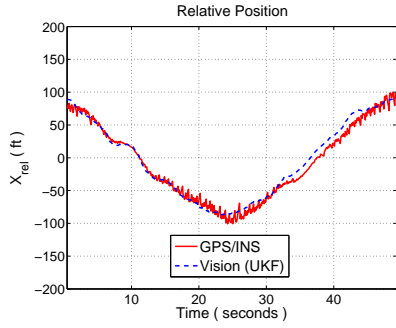
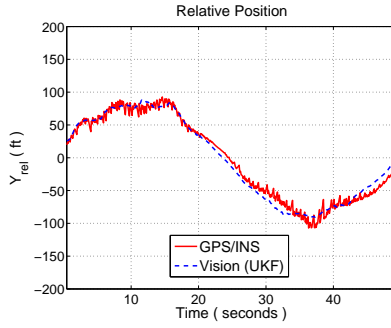


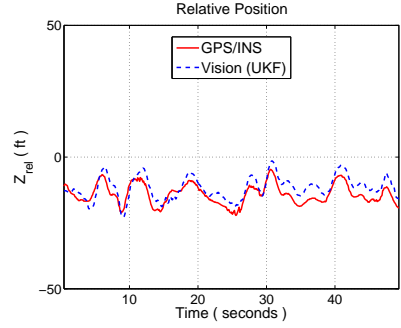
Figure 7. UKF Measurements



(a) Relative Position, X (ft)

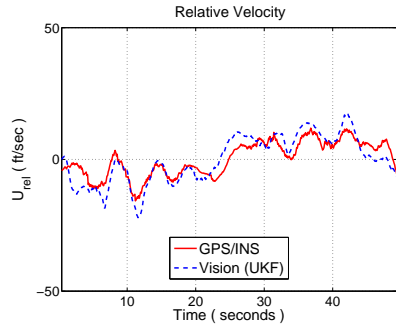


(b) Relative Position, Y (ft)

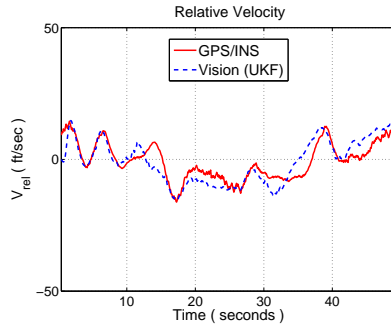


(c) Relative Position, Z (ft)

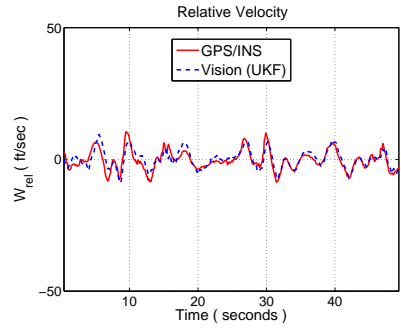
Figure 8. Relative Position



(a) Relative Velocity, U (ft/sec)

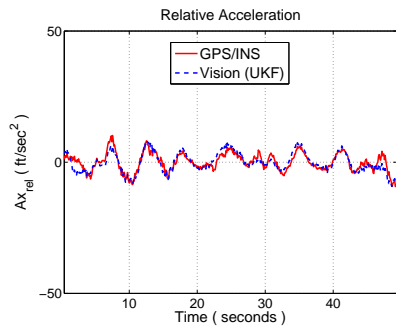


(b) Relative Velocity, V (ft/sec)

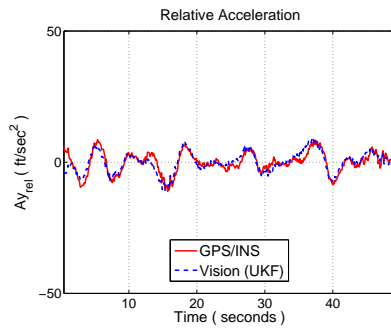


(c) Relative Velocity, W (ft/sec)

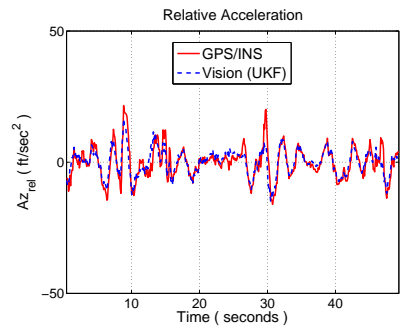
Figure 9. Relative Velocity



(a) Relative Acceleration, A_x (ft/sec^2)

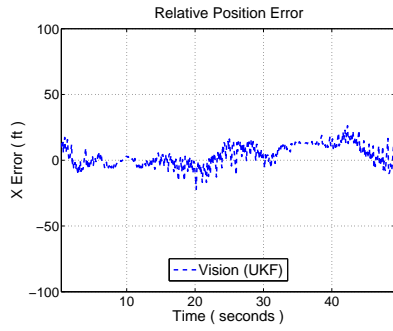


(b) Relative Acceleration, A_y (ft/sec^2)

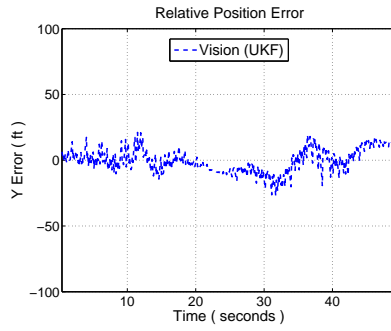


(c) Relative Acceleration, A_z (ft/sec^2)

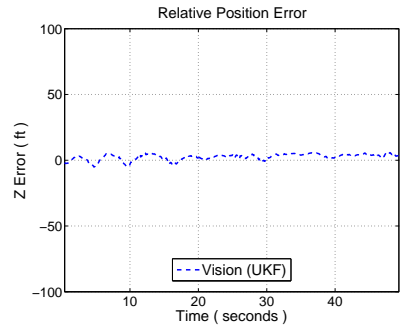
Figure 10. Relative Acceleration



(a) X Relative Position Error (ft)

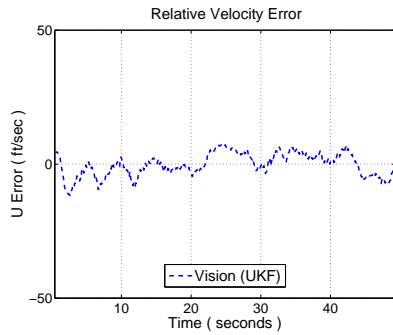


(b) Y Relative Position Error (ft)

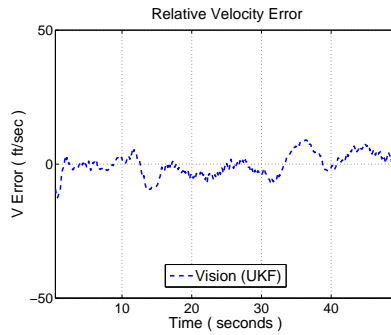


(c) Z Relative Position Error (ft)

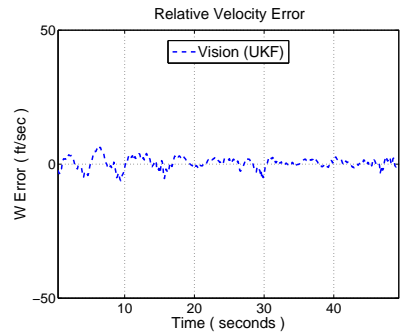
Figure 11. Relative Position Error



(a) U Relative Velocity Error (ft/sec)

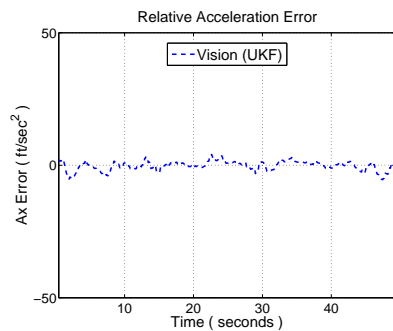


(b) V Relative Velocity Error (ft/sec)

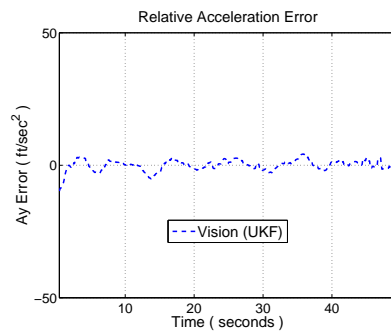


(c) W Relative Velocity Error (ft/sec)

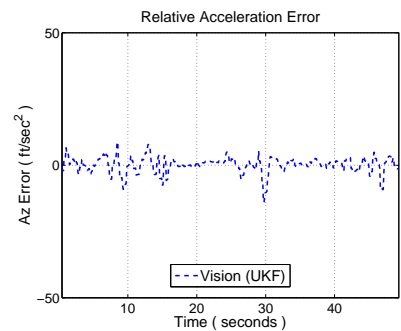
Figure 12. Relative Velocity Error



(a) A_x Relative Acceleration Error (ft/sec^2)



(b) A_y Relative Acceleration Error (ft/sec^2)



(c) A_z Relative Acceleration Error (ft/sec^2)

Figure 13. Relative Acceleration Error

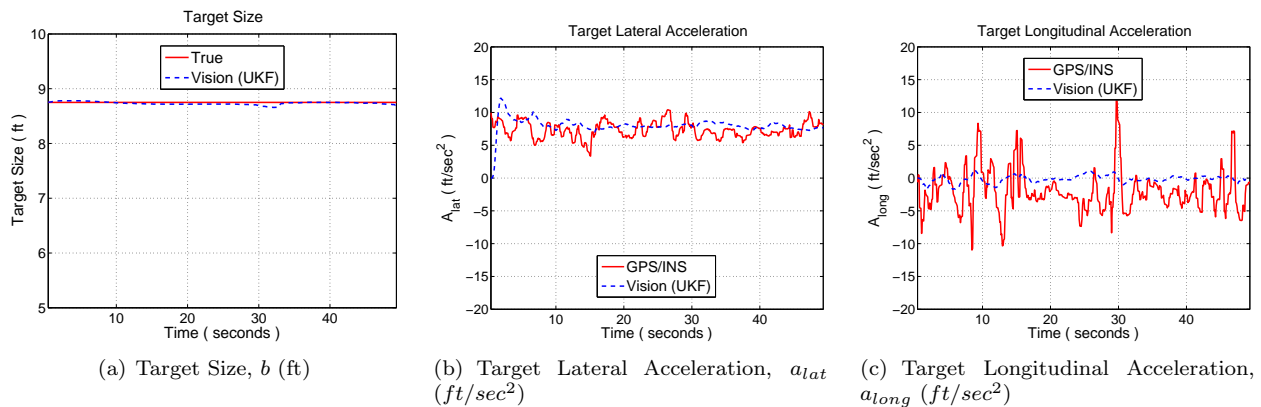


Figure 14. Target Characteristics

V. Conclusions and Future Research

This paper discusses the development of a vision-based navigation system to be used in the autonomous research UAV's. The vision-based navigation system estimates target relative kinematics and some target characteristics based on vision-only target image information in the framework of an unscented Kalman filter (UKF). The vision information for the relative motion estimator is composed of three target angles: an azimuth angle, an elevation angle, and a subtended angle. Using these measurements of vision information, the follower aircraft estimates a target relative position, a target relative velocity, a target size, and target lateral/longitudinal acceleration components using the UKF. The UKF is applied to the relative motion estimator due to the highly nonlinear characteristics of the problem at hand. By incorporating some of target characteristics such as the target size and target lateral/longitudinal accelerations as part of the estimation states, accurate estimation of the relative motion kinematics about the target is obtained. Accurate estimation of the surrounding environment (e.g., relative location/velocity of stationary or moving obstacles, relative position/velocity of friendly or enemy vehicles) can provide more probability of ownship safety and a successful mission under the circumstances of noisy and uncertain environment information.

In order to evaluate the performance of the vision-based navigation filter, vision information obtained through a real-time flight test is post-processed by the filter. The real-time vision information, obtained by a geometric active contour method on an onboard computer, is composed of three points of the target aircraft on the camera image plane. These points are the target center point, the target left wingtip point, and the target right wingtip point. The target center point on the camera image plane provides the information about the azimuth and the elevation angles of the target in the camera frame, and the two wingtip points provide information about the subtended angle of the target that provides the target size. The vision-based estimation results about the target-follower relative motion and target characteristics are compared to actual data that are independently obtained from onboard integrated navigation systems of both aircraft during a flight test. Comparisons indicate that the vision-based estimation filter provides satisfactory estimation results and thus successfully overcomes the highly nonlinear system characteristics by the UKF framework. Even though estimator performance is simulated in the scenario of a formation flight, this work can be easily applied to not only flying in formation but also avoiding or pursuing other aircraft (e.g., stationary or moving obstacle avoidance, target tracking, evasive maneuvering). In future research to get better estimation results, we may need to incorporate more sophisticated representation of target image information such as probabilistic representation instead of deterministic representation of target three points.

VI. Acknowledgement

This work was supported in part by AFOSR MURI, #F49620-03-1-0401: Active Vision Control Systems for Complex Adversarial 3-D Environments.

References

- ¹Campbell, M. E. and Wheeler, M., "A Vision Based Geolocation Tracking System for UAV's," AIAA guidance, navigation, and control conference, Aug. 2006.
- ²Langelaan, J. W., *State Estimation for Autonomous Flight in Cluttered Environments*, Ph.D. thesis, Stanford University, California, 2006.
- ³Crawford, B. G. and Downing, D. R., "Design and Evaluation of an Autonomous, Obstacle Avoiding, Flight Control System Using Simulated Visual Sensors," AIAA 3rd unmanned unlimited technical conference, 2004.
- ⁴Wagter, C. D. and Mulder, J. A., "Toward Vision-Based UAV Situation Awareness," AIAA guidance, navigation, and control conference, Aug. 2005.
- ⁵Langelaan, J. and Rock, S., "Navigation of Small UAVs Operating in Forests," AIAA guidance, navigation, and control conference, Aug. 2004.
- ⁶Oh, S.-M. and Johnson, E. N., "Development of UAV Navigation System Based on Unscented Kalman Filter," AIAA guidance, navigation, and control conference, Aug. 2006.
- ⁷Ivey, G. F. and Johnson, E. N., "Investigation of Methods for Target State Estimation Using Vision Sensors," AIAA guidance, navigation, and control conference, Aug. 2005.
- ⁸Johnson, E. N., Calise, A. J., Sattigeri, R., Watanabe, Y., and Madyastha, V., "Approaches to Vision-Based Formation Control," 43rd IEEE conference on decision and control, 2004.
- ⁹Watanabe, Y., Johnson, E. N., and Calise, A. J., "Vision-Based Guidance Design from Sensor Trajectory Optimization," AIAA guidance, navigation, and control conference, Aug. 2006.
- ¹⁰Watanabe, Y., Calise, A. J., Johnson, E. N., and Evers, J. H., "Minimum-Effort Guidance for Vision-Based Collision Avoidance," AIAA guidance, navigation, and control conference, Aug. 2006.
- ¹¹Proctor, A. A. and Johnson, E. N., "Vision-Only Approach and Landing," AIAA guidance, navigation, and control conference, Aug. 2005.
- ¹²Proctor, A. A. and Johnson, E. N., "Vision-Only Aircraft Flight Control Methods and Test Results," AIAA guidance, navigation, and control conference, Aug. 2004.
- ¹³Kurdila, A., Nechyba, M., Prazenica, R., Dahmen, W., Binev, P., DeVore, R., and Sharpley, R., "Vision-Based Control of Micro-Air-Vehicles: Progress and Problems in Estimation," 43rd IEEE conference on decision and control, 2004.
- ¹⁴Watanabe, Y., Johnson, E. N., and Calise, A. J., "Vision-Based Approach to Obstacle Avoidance," AIAA guidance, navigation, and control conference, Aug. 2005.
- ¹⁵Johnson, E. N., Calise, A. J., Watanabe, Y., Ha, J., and Neidhoefer, J. C., "Real-Time Vision-Based Relative Navigation," AIAA guidance, navigation, and control conference, Aug. 2006.
- ¹⁶Johnson, E. N., Calise, A. J., Tannenbaum, A. R., Soatto, S., Hovakimyan, N., and Yezzi, A. J., "Active-Vision Control Systems For Complex Adversarial 3-D Environments," A tutorial, IEEE american control conference, 2005.
- ¹⁷Sattigeri, R., Calise, A. J., Kim, B. S., Volyanskyy, K., and Kim, N., "6-DOF Nonlinear Simulation of Vision-based Formation Flight," AIAA guidance, navigation, and control conference, Aug. 2005.
- ¹⁸Ristic, B., Arulampalam, S., and Gordon, N., "Chapter 6. Bearings-Only Tracking," *Beyond the Kalman Filter: Particle Filters for Tracking Applications*, Artech House, Boston, 2004, pp. 103–151.
- ¹⁹Cui, S.-H. and Zhu, C.-Q., "Application of Kalman Filter to Bearing-Only Target Tracking System," International conference on signal processing, ICSP 1996, 1996.
- ²⁰Lerro, D. and Bar-Shalom, Y., "Bias Compensation for Improved Recursive Bearings-Only Target State Estimation," American control conference, 1995.
- ²¹Aidala, V. J. and Hammel, S. E., "Utilization of Modified Polar Coordinates for Bearings-Only Tracking," *IEEE Transactions on Automatic Control*, , No. 3, 1983, pp. 283–294.
- ²²Xu, Y. and Liping, L., "Single Observer Bearings-Only Tracking with the Unscented Kalman Filter," International conference on communications, circuits and systems, ICCAS 2004, 2004.
- ²³Gordon, N. J., Salmond, D. J., and Smith, A. F. M., "Novel approach to nonlinear/non-Gaussian Bayesian state estimation," *IEE Proceedings F on Radar and Signal Processing*, 1993, pp. 107–113.
- ²⁴Wan, E. A. and van der Merwe, R., "Chapter 7. The Unscented Kalman Filter," *Kalman Filtering and Neural Networks*, edited by S. Haykin, John Wiley & Sons, New York, 2001.
- ²⁵Julier, S. J. and Uhlmann, J. K., "A New Extension of the Kalman Filter to Nonlinear Systems," Proc. of aerosense: The 11th int. symp. on aerospace/defense sensing, simulation and controls, Aug. 1997.
- ²⁶van der Merwe, R. and Wan, E. A., "Sigma-Point Kalman Filters for Probabilistic Inference in Dynamic State-Space Models," Workshop on advances in machine learning, 2003.
- ²⁷Koch, A., Wittich, H., and Thielecke, F., "A Vision-Based Navigation Algorithm for a VTOL-UAV," AIAA guidance, navigation, and control conference, Aug. 2006.
- ²⁸Roderick, A. R., Kehoe, J. J., and Lind, R., "Vision-Based Navigation using Multi-Rate Feedback from Optic Flow and Scene Reconstruction," AIAA guidance, navigation, and control conference, Aug. 2005.
- ²⁹Webb, T. P., Prazenica, R. J., Kurdila, A. J., and Lind, R., "Vision-Based State Estimation for Uninhabited Aerial Vehicles," AIAA guidance, navigation, and control conference, Aug. 2005.
- ³⁰Fosbury, A. M. and Crassidis, J. L., "Kalman Filtering for Relative Inertial Navigation of Uninhabited Air Vehicles," AIAA guidance, navigation, and control conference, Aug. 2006.
- ³¹Johnson, E. N. and Schrage, D. P., "The Georgia Tech Unmanned Aerial Research Vehicle: GTMax," AIAA guidance, navigation, and control conference, Aug. 2003.
- ³²Johnson, E. N. and Schrage, D. P., "System Integration and Operation of a Research Unmanned Aerial Vehicle," *AIAA Journal of Aerospace Computing, Information, and Communication*, Vol. 1, No. 1, Jan. 2004.

³³Dittrich, J. S. and Johnson, E. N., "Multi-sensor Navigation System for an Autonomous Helicopter," Proceedings of the 21st digital avionics systems conference.

³⁴Dittrich, J. S., "Design and Integration of an Unmanned Aerial Vehicle Navigation System," M.s. thesis, georgia institute of technology, May 2002.

³⁵Shaviv, I. G. and Oshman, Y., "Guidance Without Assuming Separation," AIAA guidance, navigation, and control conference, Aug. 2005.

³⁶Julier, S. J., Uhlmann, J. K., and Durrant-Whyte, H., "A New Approach for Filtering Nonlinear Systems," Proceedings of the american control conference, Seattle, WA, 1995.

³⁷Julier, S. J., Uhlmann, J. K., and Durrant-Whyte, H., "A New Method for the Nonlinear Transformation of Means and Covariances in Filters and Estimators," *IEEE Transactions on Automatic Control*, , No. 3, 2000, pp. 477–482.

³⁸van der Merwe, R. and Wan, E. A., "Sigma-Point Kalman Filters for Nonlinear Estimation and Sensor-Fusion - Application to Integrated Navigation," AIAA guidance, navigation, and control conference, Aug. 2004.

³⁹van der Merwe, R. and Wan, E. A., "The Square-Root Unscented Kalman Filter for State and Parameter-Estimation," Proceedings of the IEEE international conference on acoustics, speech, and signal processing (icassp), May 2001.